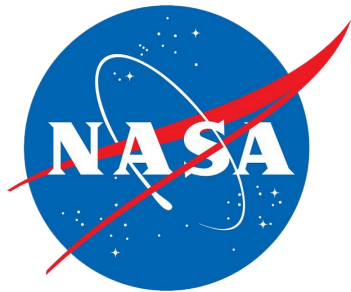
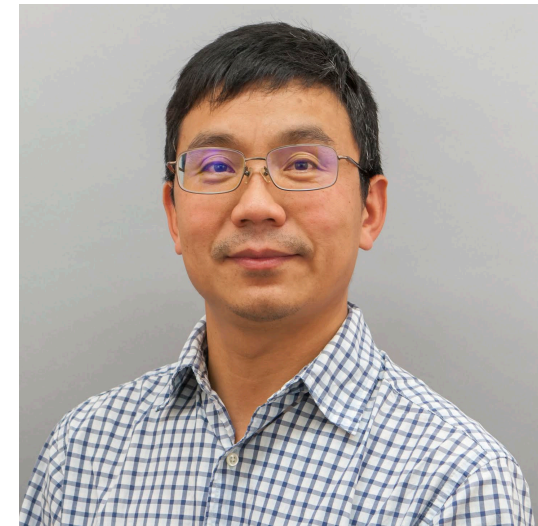


# Seasonality of $M_2$ Internal Tides Observed by Satellite Altimetry

Zhongxiang Zhao

Applied Physics Laboratory, University of Washington

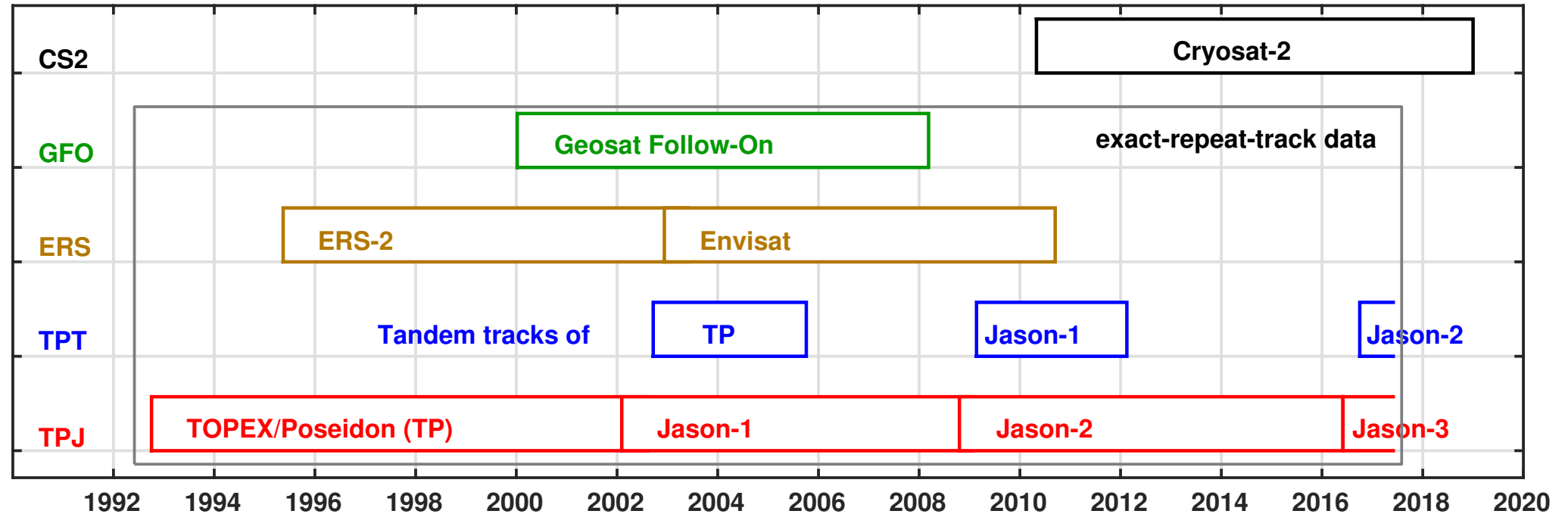


OSTST 2020 Virtual Forum

# Abstract

The seasonal variation of  $M_2$  internal tides is investigated using 25 years of satellite altimeter sea surface height measurements from 1992–2017. This study employs a new five-step mapping technique that combines along-track high-pass filtering, harmonic analysis, plane wave analysis, and two-dimensional bandpass filtering. The altimeter data are divided into four seasonal subsets, from which four seasonal  $M_2$  internal tide models are constructed by the same mapping technique. Two time-mean models are constructed. The first one is the 25-year-coherent model constructed using all the data following the same procedure. The second one is the seasonal-mean model obtained from the vector mean of the four seasonal models. Two seasonally-variable models are derived. The first model is a step function of the four seasonal models (i.e., variable amplitude and phase). The second model is same as the first model but that its amplitude is the seasonal vector mean (i.e., variable phase and invariable amplitude). These eight models are inter-compared, and evaluated using nine years of CryoSat-2 data. The results show that the seasonal-mean and 25-year-coherent models are equivalent. The four seasonal models have larger uncertainties, because of their short seasonal data records. The four seasonal models reduce less variance than the 25-year-coherent model. Each of these seasonal models reduces the most variance in its respective season when they are evaluated using seasonally subsetting CryoSat-2 data. The seasonally-variable models may reduce more variance in the equatorial zone, and the second seasonally-variable model works better than the first one. Direct point-wise comparisons of these models reveal significant seasonal variation in regions including the equatorial zone ( $\pm 90$  degrees in phase), the Amazon River mouth, the west Pacific, and the Arabian Sea. In regions such as the Northeast Pacific, the seasonal variation is detectable though weak. In conclusion, (1) the global  $M_2$  internal tides are subjected to significant seasonal variation, (2) the seasonal variation is a function of location, and (3) a fraction of the seasonal variation can be corrected by seasonally-variable internal tide models.

# Data



Seasonal  $M_2$  internal tide models are constructed using 25 years of satellite sea surface height data from 1992–2017. The altimeter data are divided into four seasonal subsets, from which four seasonal models are constructed by the same mapping technique. The models are developed using data from exact-repeat-track missions, and evaluated using independent data from CryoSat-2.

## Eight Mode-1 $M_2$ Internal Tide Models

Model	Altimeter dataset or method	Note
Zhao20† ‡	all-year all-month	25-year-coherent
Zhao20SN1	January, February, March	winter
Zhao20SN2	April, May, June	spring
Zhao20SN3	July, August, September	summer
Zhao20SN4	October, November, December	fall
Zhao20SN0‡	vector mean of four seasonal models	seasonal-mean
Zhao20SNa	a step function of four seasonal models	phase-variable, amplitude-variable
Zhao20SNb	as Zhao20SNa but amplitudes from Zhao20SN0	phase-variable, amplitude-invariable

The first five models are constructed directly from respective satellite altimeter datasets.

The last three models are derived from the four seasonal models.

† Zhao20 is same as Zhao19b in Zhao (2019 JGR), but for in windows of 250 km (vs 160 km).

‡ The seasonal-mean and 25-year-coherent models are equivalent (almost the same).

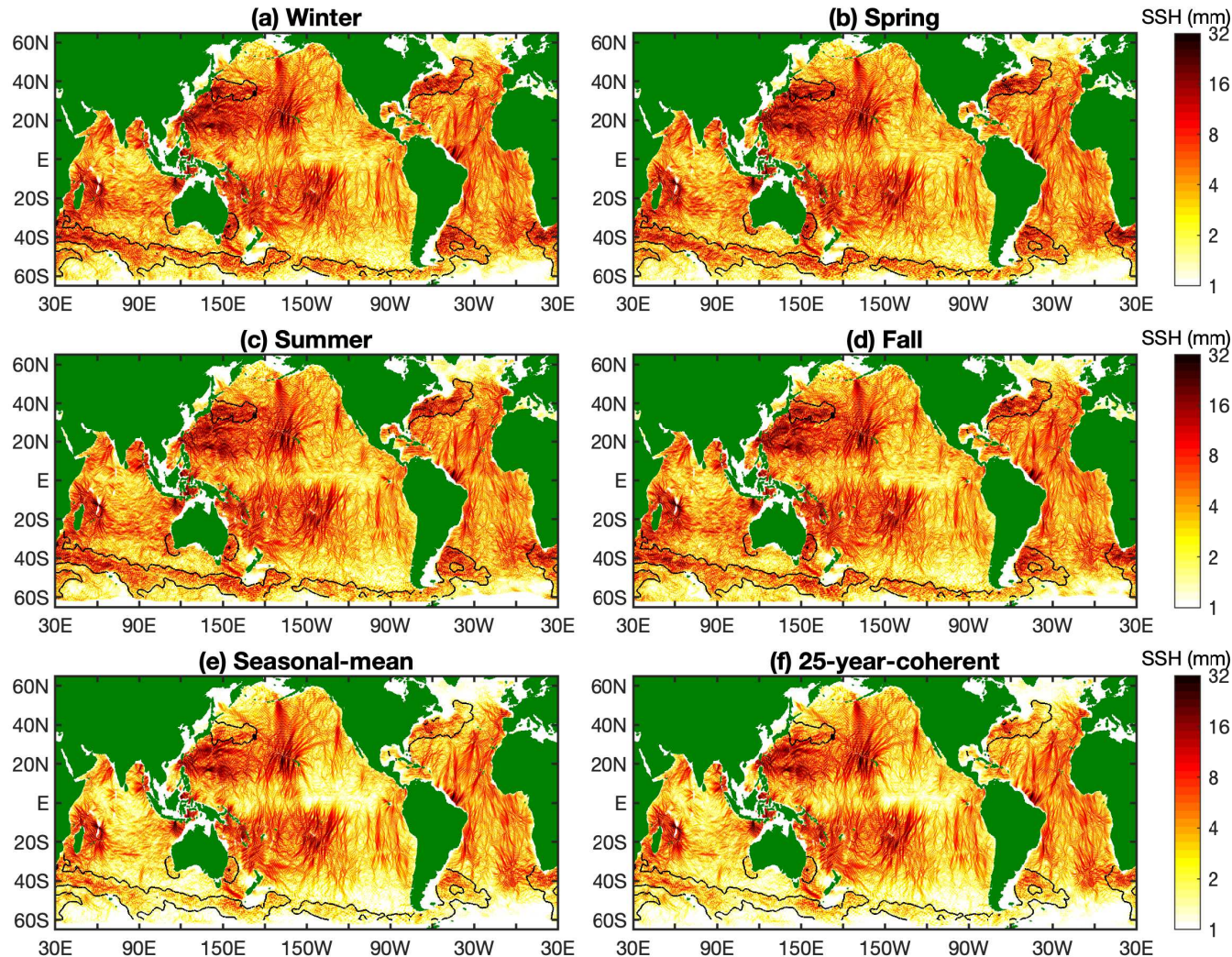
# Mapping Procedure

Step	Operation	Goal	Parameters
1	along-track high-pass filter	suppress large-scale nontidal noise	cutoff at 2000 km
2	harmonic analysis	suppress nontidal noise by tidal frequency	on track, point by point
3	plane wave analysis	map internal tides at regular spatial grid	250 km, 5 waves, $K$
4	2-D bandpass filtering	clean internal tides by wavenumber	$[0.8 \ 1.25] \times K$
5	plane wave analysis	separate internal tides by propagation direction	160 km, 5 waves, $K$

The five-step mapping procedure is presented in Zhao (2019 JGR, doi: [10.1029/2019JC015507](https://doi.org/10.1029/2019JC015507)). The goal and key parameters in each step are listed here. Theoretical wavenumber  $K$  is used in Steps 3–5. Theoretical wavenumbers (a function of location and season) are computed from the WOA13 seasonal climatology.



# Global Mode-1 $M_2$ Internal Tide Models



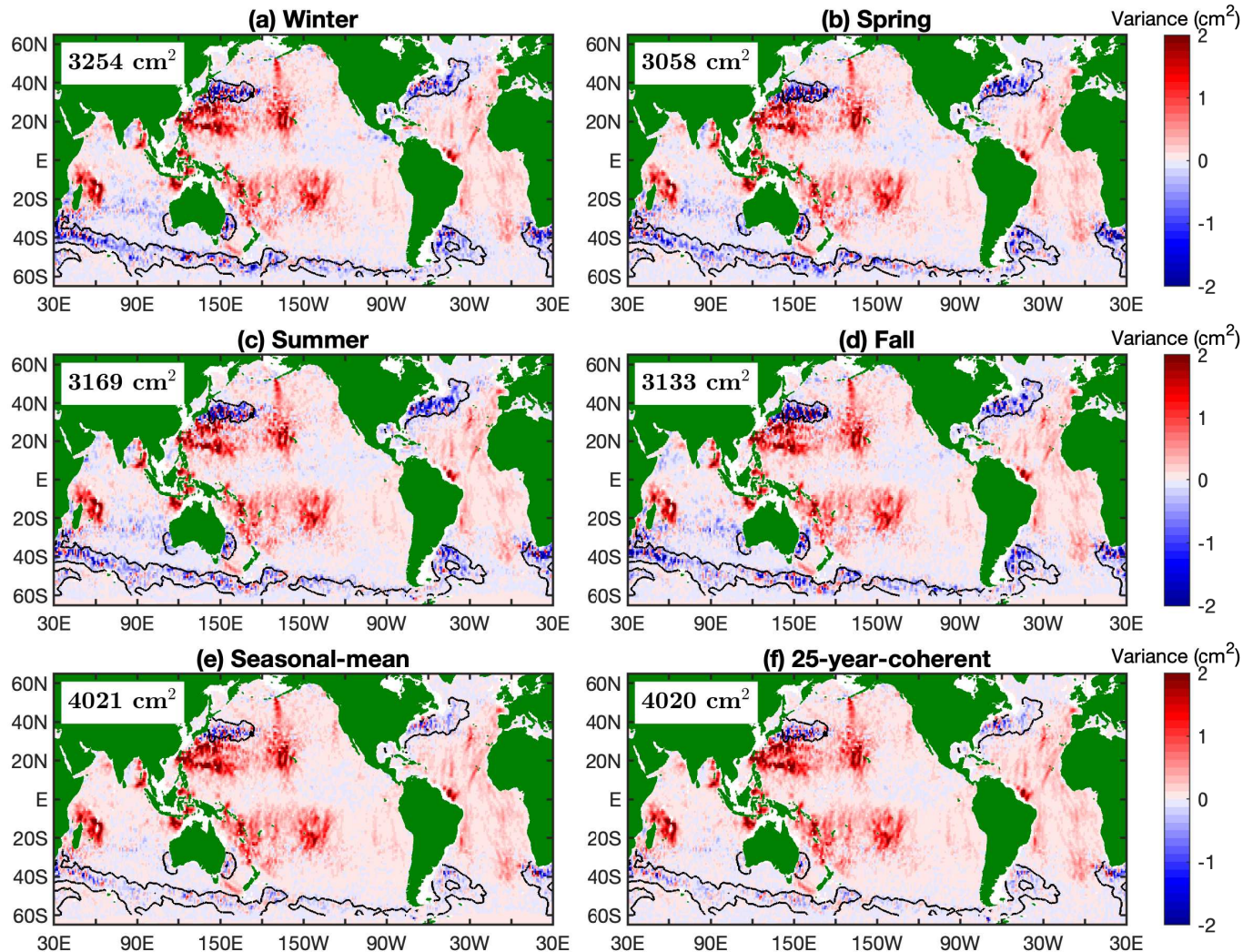
Global mode-1  $M_2$  internal tide models from satellite altimetry. Shown is the sea surface height amplitude in logarithmic scale. The black contours indicate regions of strong boundary currents, where the models are not reliable.

These models look very similar, suggesting that the internal tide field is overall stationary. However, there are significant and detectable seasonal differences as shown next.

The seasonal models have higher noise levels, due to short seasonal data records.



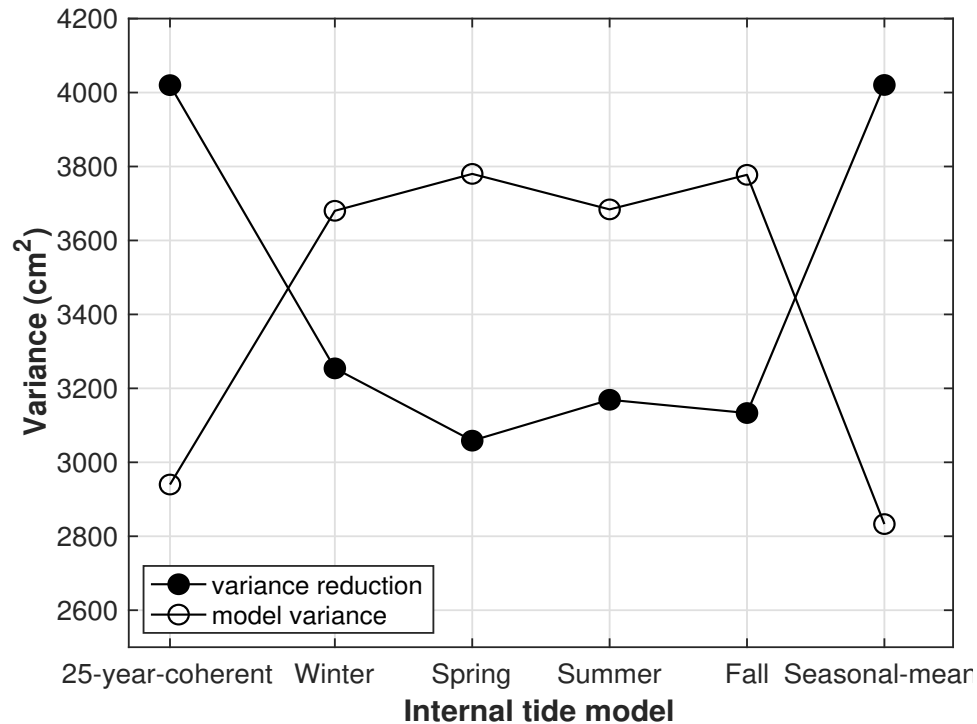
# Variance Reduction with CryoSat-2 Data



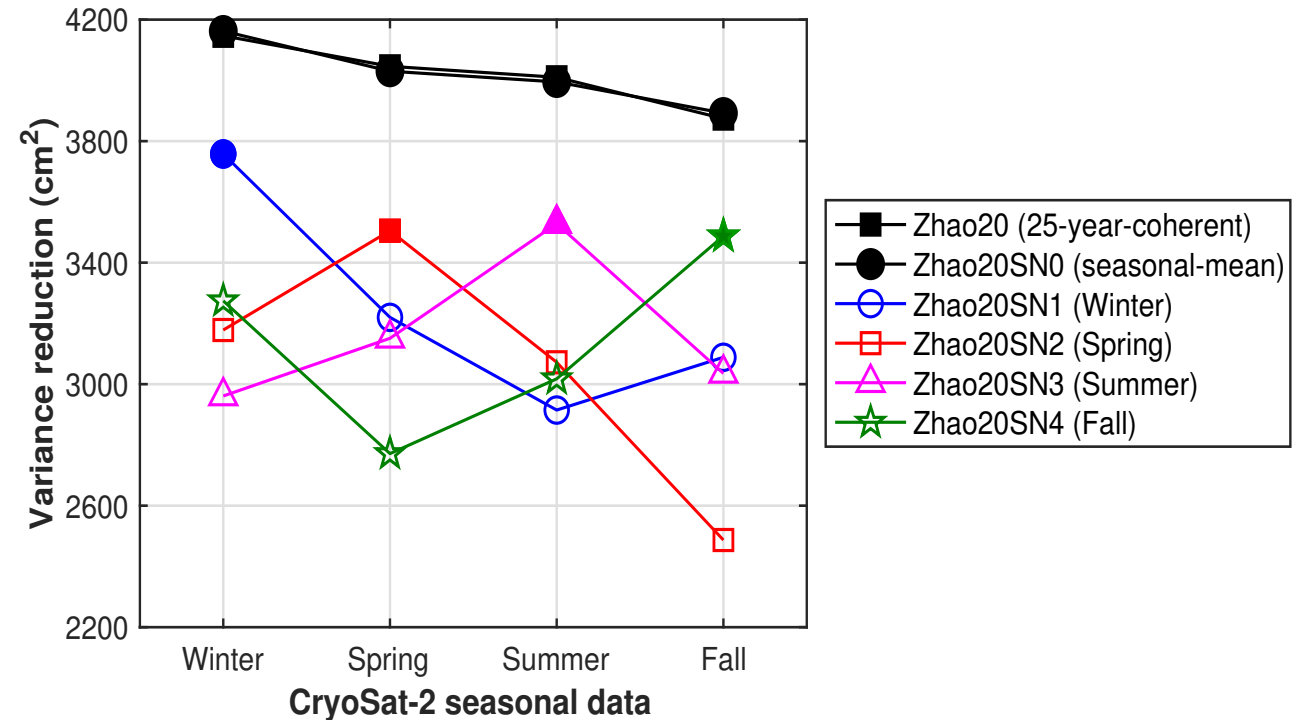
Variance reduction obtained by making internal tide correction to nine years of Cryosat-2 data. Shown is variance reduction in bins of  $2^\circ$  lon by  $2^\circ$  lat. Positive and negative values denote variance reduction and increase, respectively. The number gives the globally-integrated area-weighted variance reduction. The black contours indicate regions of strong boundary currents, where are excluded from the global integration.

The seasonal-mean and 25-year-coherent models reduce more variances than the seasonal models do.

# Model Variance and Variance Reduction



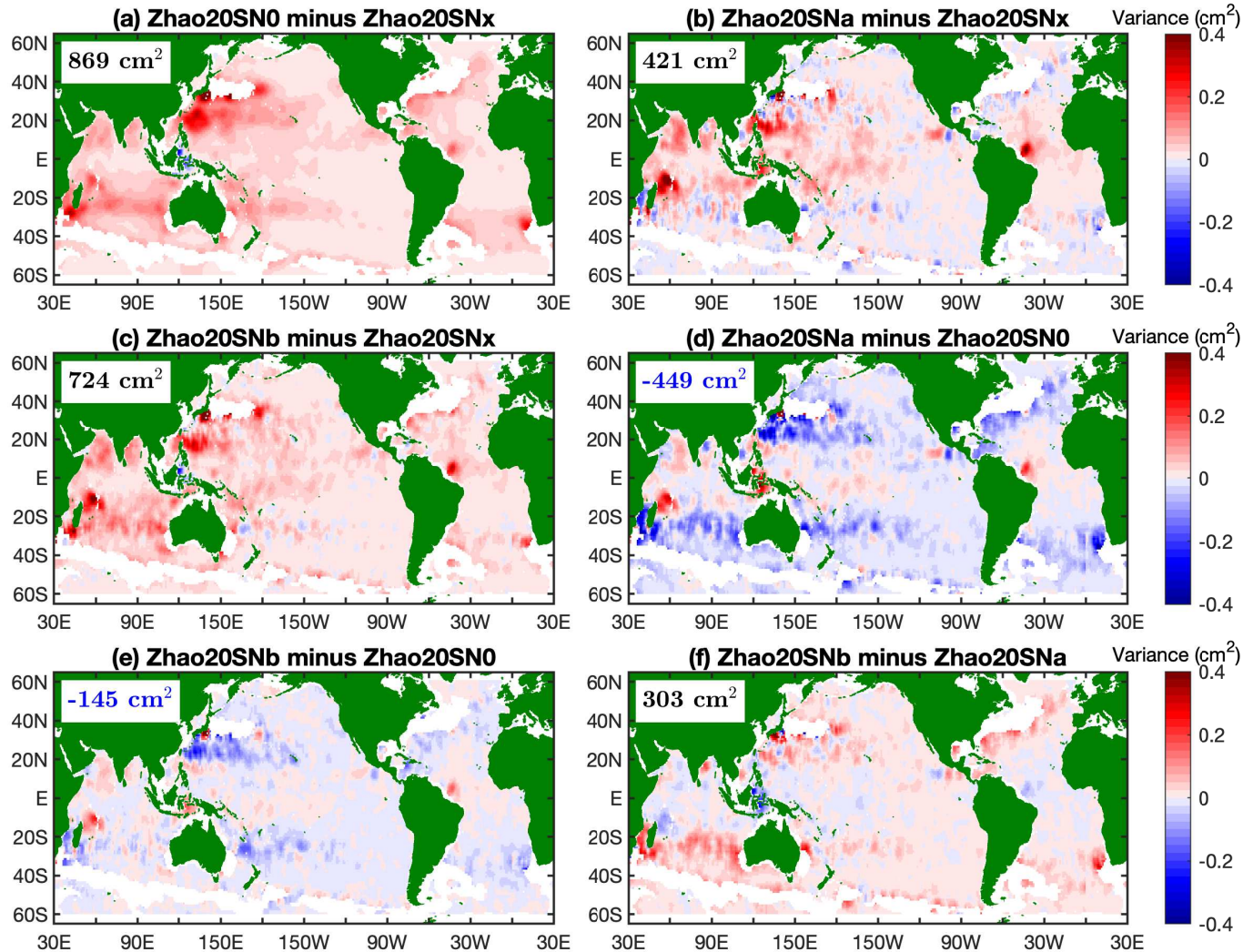
Comparison of globally integrated model variances and variance reductions for six internal tide models. The seasonal-mean and 25-year-coherent models are better, because they have low model variances and high variance reductions.



Global integration of variance reduction obtained by making internal tide correction to Cryosat-2 seasonal subsets. The four seasonal models reduce most variances in their respective seasons (filled color symbols). However, due to large nontidal noise, they reduce less variance than the time-mean models do.



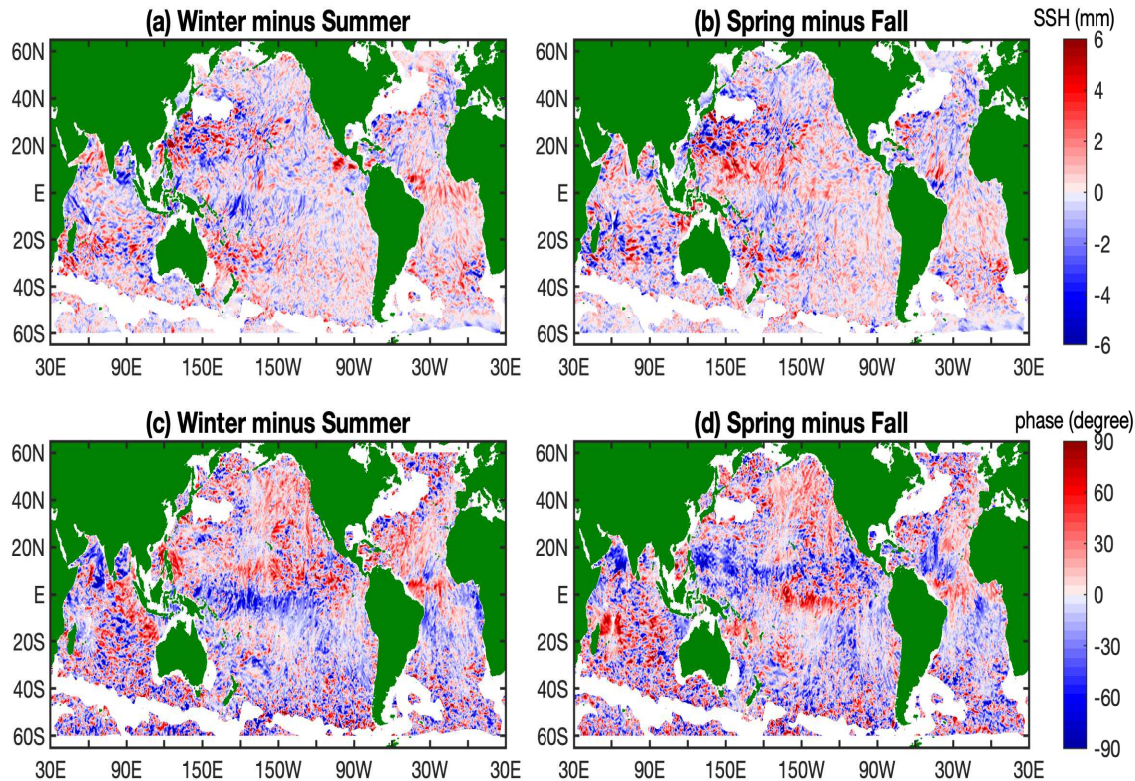
# Comparison of Variance Reductions



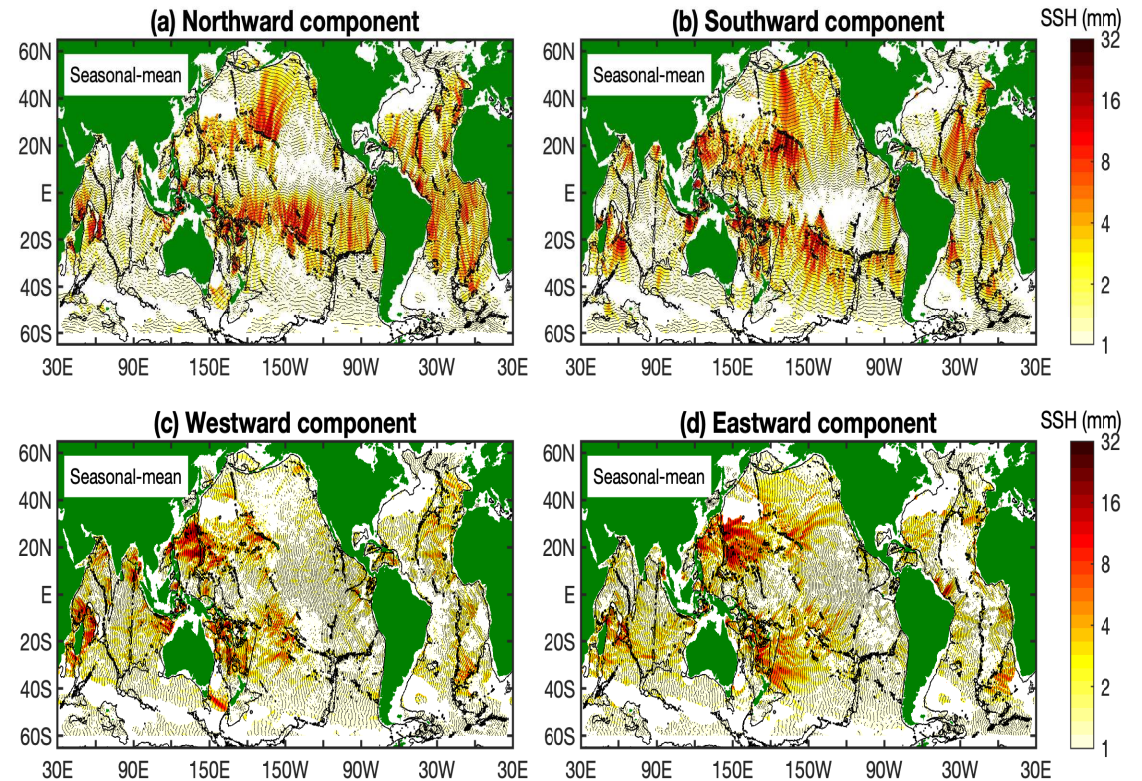
Geographic differences between variance reductions. Six pairs of internal tide models are compared as labeled. These models are described earlier, except that Zhao20SNx denotes the mean variance reduction of the four seasonal models. The globally integrated differences are given in boxes. Among them, Zhao20SNx is the worst, because they have large nontidal noise. The seasonally variable models are the best in the equatorial zone (d, e), suggesting that seasonal variation can be partially modeled and corrected. The limitation factor is the large nontidal noise (a function of location) as a result of short seasonal records.



# Seasonal Differences and Multidirectional Decomposition



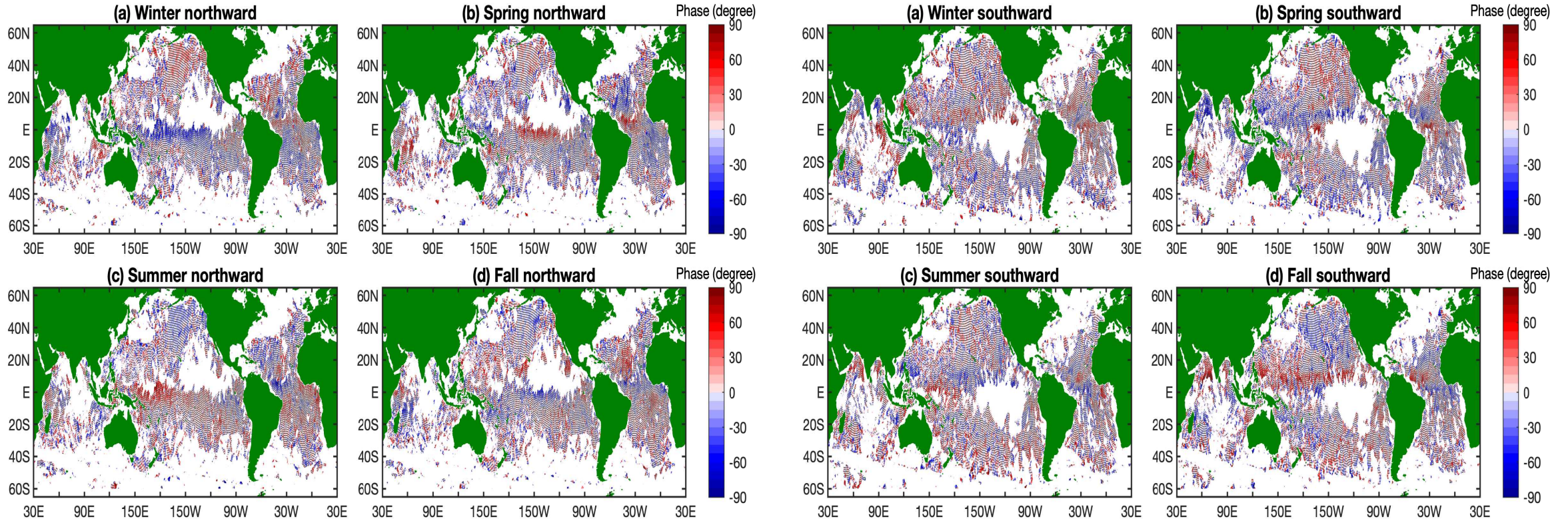
Point-wise amplitude and phase differences between (a, c) Winter and Summer, and (b, d) Spring and Fall. Significant differences can be seen in the equatorial zone, the Arabian Sea, the Amazon River mouth, the western Pacific, and so on.



Each model can be decomposed into four components of 90° directional sector (northward is 45°–135°). The amplitude is in logarithmic scale (colors). The co-phase chart is in gray line. The 3000-m isobath contours are in black line.



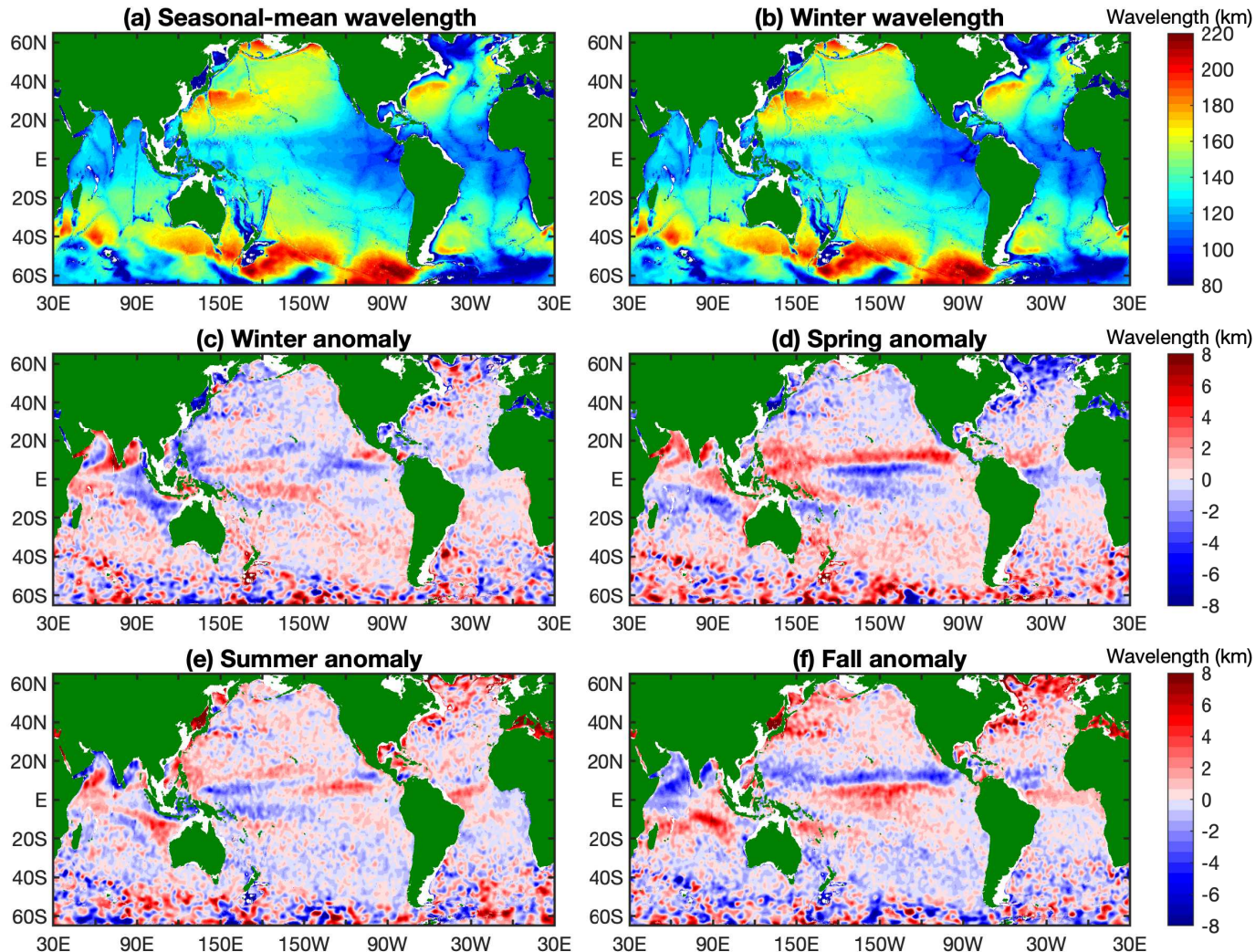
# Seasonal Phase Anomalies



Seasonal phase anomalies with respect to the seasonal-mean model. (left) Northward component ( $45^\circ$ – $135^\circ$ ). (right) Southward components ( $225^\circ$ – $315^\circ$ ). They are 5-point-smoothed point-wise differences. Regions of strong currents are not shown. Internal tides with amplitudes lower than 1 mm are not shown. Black lines show the co-phase chart. The phase anomalies in the equatorial zone are about  $\pm 90^\circ$ . The largest anomalies are in the Arabian Sea ( $\pm 180^\circ$ ). Weak seasonal phase variation in the Northeast Pacific can be seen.



# Anomalies of Seasonal wavelengths in WOA13



Ed's question: "... about the phases shown on the left side of slide 9. It looks like the phase differences are coherent over large areas near the equator. Do you understand why this is?"

ZZ's reply: "Yes. The wavelength (wave speed) of mode-1  $M_2$  internal tides has a strong seasonal cycle, due to the seasonal variation of ocean stratification. Based on WOA13, the seasonal wavelength anomalies may be  $\pm 8$  km near the equator (left figure). The coherent phase anomaly patterns are mainly caused by seasonally different wavelengths (wave speeds)."



Questions? Comments? Suggestions?

Please contact me at [zzhao@apl.uw.edu](mailto:zzhao@apl.uw.edu)

Thank you very much for your attention!